Structural Determination of Oxofatty Acids by Charge-Remote Fragmentations

Changfu Cheng, Daryl Giblin, and Michael L. Gross
Department of Chemistry, Washington University, St. Louis, Missouri, USA

A strategy is described to locate the carbonyl position in oxofatty acids by utilizing charge-remote fragmentations of various molecular ions that are desorbed by fast atom bombardment (FAB). Oxofatty acids were cationized with alkali metal ions (Li^+, Na^+, K^+, Rb^+, and Cs^+) to form $[M+2Met - H]^+$ or alkaline earth metal ions (Mg^{2+}, Ca^{2+}, Sr^{2+} or Ba^{2+}) to form $[M+Met-H]^+$ in the gas phase. The cationized acids undergo charge-remote fragmentations upon high-energy activation, giving a product-ion pattern that has a gap corresponding to the oxo position and bordered by two high-intensity peaks. One of the peaks corresponds to an ion that is formed by the cleavage of the C–C bond β to the oxo position and proximal to the charge (β ion), whereas the other is formed from the cleavage of the C–C bond γ to the oxo position and distal to the charge (γ' ion). The oxo position is easily determined by identifying the gap and the β and γ' ions. Furthermore, there are two competing patterns of fragments in a CAD spectrum of an oxofatty acid or ester $[M+Li]^+$ ion. These arise because Li^+ attaches to either the oxo or the carboxylic end, as was confirmed by ab initio molecular orbital calculations. The results demonstrate that control of the fragmentation can be guided by an understanding of metal-ion affinities. Collisional activation of the anionic carboxylates gives results that are similar to those for positive ions, showing that the process is not related to the charge status. Collisional activation of $[M+H]^+$ ions does not give structural information because the charge migrates, leading to charge-mediated fragmentations. (J Am Soc Mass Spectrom 1998, 9, 216–224) © 1998 American Society for Mass Spectrometry

Long-chain alkyl compounds, including fatty acids and their esters, fatty alcohols, surfactants, phosphonium salts, and vitamins can be structurally characterized by high-energy collisional activation and tandem mass spectrometry (MS/MS) [1]. Sample molecules that are desorbed by fast atom bombardment (FAB) as $[M+Met]^+$, where Met is an alkali-metal ion (Li^+, Na^+, K^+, Rb^+ or Cs^+), or as $[M-H+Met]^+$, where *Met* is an alkaline earth metal ion (Mg^{2+}, Ca^{2+}, Sr^{2+} or Ba^{2+}) [2] or by deprotonation, undergo decompositions that occur remote from charge sites and are analogous to thermolytic processes; thus, the name charge-remote fragmentations. These processes are high-energy, gas-phase dissociations that, when occurring along an alkyl chain, involve losses of the elements of C_nH_{2n+2} through a 1,4-hydrogen elimination mechanism as proposed by Jensen et al. [3] and verified recently by Wesdemiotis and co-workers [4] (see eq 1).

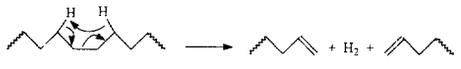

(1)

A "fixed" charge site is essential for obtaining a distinctive pattern of charge-remote product ions. Protonated fatty alcohols and fatty acids do not fragment by the 1,4-elimination mechanism to produce structurally informative product ions when the charge is not fixed [5, 6]. For example, $[M+H]^+$ ions lose small neutral molecules such as H_2O to generate carbocations that subsequently undergo charge-driven fragmentations [7]. In special circumstances, the proton can be strongly bonded to a polar functional group, and charge-remote fragmentation can be induced [8]. Even the fragmentations of carboxylates, to some extent, have similar problems because they lose CO_2 when a stable anion can form and undergo charge-driven in lieu of charge-remote fragmentations, making data interpretation difficult [9].

High-energy collisional activation has been successfully applied to determine locations of one or several double bonds, cyclopropane, cyclopropene or epoxide rings, alkyl or hydroxyl substituents in fatty acids and related compounds [1b, c]. Moreover, the method may be used to elucidate structures of certain complex lipids because lipids dissociate to give carboxylates that can be determined by MS/MS.

The oxofatty acid esters were investigated under EI conditions and isomers were distinguishable by identifying ions from McLafferty rearrangement and acylium ions from α-cleavage to the keto [10]. Because the charge-remote fragmentations of oxofatty acids have

Address reprint requests to Dr. M. L. Gross, Department of Chemistry, Washington University, One Brookings Drive, Box 1134, St. Louis, MO 63130. E-mail: mgross@wuchem.wustl.edu

1044-0305/98/$19.00
PII S1044-0305(97)00283-3

Received September 3, 1997
Revised November 7, 1997
Accepted November 10, 1997

not been studied by MS/MS, we report here a systematic study of these acids and show that these fragmentations can locate the oxo position in a fatty acid chain and, therefore, distinguish oxofatty acid isomers that are otherwise difficult to discriminate by means of NMR and optical spectroscopy. An additional motivation comes from a recent study of extracts from the marine sponge *Pellina triangula* where we were unable to interpret with confidence the CAD spectrum of a lipid material containing an oxo group [11].

Experimental

Reagents

Matrix compounds, including 3-nitrobenzyl alcohol (3-NBA), glycerol, diethanolamine (DEA), triethanolamine (TEA), LiI, NaI, KBr, RbI, CsI, $MgCl_2$, $CaCl_2$, $Sr(NO_3)_2$, and $BaCl_2$ were purchased from either Aldrich (Milwaukee, WI) or Sigma (St. Louis, MO). The compounds, 10-oxoundecanoic, 13-oxopentadecanoic, 10-oxohexadecanoic, 13-oxooctadecanoic, 7-oxotetracosanoic and 13-oxotetracosanoic acids, 2,3-dihydroxypropyl 4-oxostearate, *p*-hexadecanoacetanisidine, and *N*-[(2-methylamino)ethyl]-2-oxononadecanamide, were obtained from Sigma-Aldrich Library of Rare Chemicals (Milwaukee, WI).

4-Oxooctadecanoic acid was obtained by refluxing 2,3-dihydroxypropyl-4-oxostearate in acetone with a few drops of dilute sulfuric acid for 30 min. 2-Oxotetradecanoic acid was synthesized by oxidizing the methyl ester of 2-hydroxytetradecanoic acid (Phase Separations, Norwalk, CT) with excess pyridinium chlorochromate (PCC) (Sigma) in CH_2Cl_2 for 2 h at room temperature. 16-Oxohexadecanoic acid was produced by refluxing 16-hydroxyhexadecanoic acid (Sigma) in CH_2Cl_2 with excess PCC for 30 min. 12-Oxooctadecanoic acid was obtained by refluxing methyl 12-hydroxyoctadecanoate with excess PCC for 1 h followed by hydrolyzing the ester with KOH in acetone. The crude product was dissolved in CH_2Cl_2, washed in separate steps with H_2O, 5% HCl, and H_2O, dried over $MgSO_4$, and the solvent evaporated in vacuum. The purified products were desorbed as $[M+H]^+$ by FAB, and their exact masses were measured at a resolving power of 10,000; the exact masses of all synthetic products were within 5 ppm of their theoretical values.

Instrumentation and Procedures

The first-round experiments were performed with a Kratos (Manchester, England) MS-50 triple analyzer tandem mass spectrometer [12]. The resolving power of MS1 was approximately 2500, whereas that of MS2 was limited to approximately 100 by the peak broadening caused by the kinetic energy released upon fragmentation. Negative-ion experiments were carried out by using TEA or DEA as matrix, and positive-ion experiments by using 3-NBA saturated with a metal halide salt as matrix. In a typical experiment, a small amount (~1 μg) of a fatty acid was mixed with the matrix on the FAB tip and bombarded with a 6-keV Ar beam at an initial gun current of 2 mA. The ions were then accelerated to 8-keV translational energy, selected by MS1, and activated by colliding them with helium gas in a grounded collision chamber between MS1 and MS2 (laboratory kinetic energy of 8 keV). The amount of helium was controlled to give a 50% attenuation of the selected ion beam. Product-ion spectra were generated by scanning MS2 and averaging the data from 10–40, 20-s scans.

Higher resolving power product-ion spectra were obtained with a ZAB-T four-sector tandem mass spectrometer manufactured by VG Analytical (Manchester, England), which was described elsewhere [13]. For MS/MS experiments, ions were formed by bombarding the sample and matrix described above with a high-energy (~25 keV) Cs^+ ion beam. The ions were accelerated to 8-keV kinetic energy, selected by the first stage (MS1) at a mass resolving power of ~1500, and collided with helium in the collision cell, which was between MS1 and MS2 and floated to 4 kV (laboratory kinetic energy of 4 keV). The product ions were analyzed by scanning MS2 which was operated at a mass resolving power of ~1000 (full width at half-maximum). Product-ion spectra were obtained by averaging the data from approximately 30 15-s scans.

Ab Initio Calculations

All calculations involving geometric optimization and energy and frequency calculations were carried out by using the Gaussian 94 suite of programs [14], which were run on a Silicon Graphics Power Challenge workstation. Spartan v.4 (Wavefunction, Inc., Irvine, CA), which was running on a Silicon Graphics Indigo II workstation, was employed as a graphical front end for Gaussian 94 for most calculations.

The interactions of H^+, Li^+, and Na^+ with the functional groups of the oxofatty acids were modeled by theoretical calculations of the attachment products of these cations with formaldehyde, formate anion, and methyl formate. Candidate structures for each of the various adducts and reactants (except cations) were optimized by using the self-consistent field (SCF-HF) method with the 6-31G(d) basis set for all atoms [HF/6-31G(d)]. All stationary points of a given species having energies within ~5 kcal/mol of the form with the lowest energy were subjected to further geometric refinement by the MP2 method over all electrons with the 6-31+G(d) as basis set [MP2(Full)/6-31+G(d)]. The vibrational frequencies at this level of optimization were calculated and used to confirm the stationary points as minima. In addition, thermal-energy corrections to attain standard conditions (temperature 298.15 K; pressure 1 atm) were calculated at this level from scaled zero-point energies and fundamental vibrational frequencies and used to correct all further calculations

[15]. Corrected energies of all species thus qualified as minima were calculated from the energies derived from a final round of geometric optimization performed at the level of MP2(Full)/6-311+G(2d,p) and the thermal-energy corrections. The lowest-energy form of each species was then used in the reaction calculations. The energies of cations, Li^+ and Na^+, were simply calculated at the level, MP2(Full)/6-311+G(2d,p). Detachment energies and cation affinities, the negative of reaction energies and enthalpies, respectively, of the attachment reactions, were evaluated from the corrected energies with the assumption of an ideal gas for the reaction-enthalpy calculations.

Results and Discussion

General Features of the CAD Spectra of Oxofatty Acids

Fast atom bombardment (FAB) of oxofatty acids in 3-nitrobenzyl alcohol saturated with LiI produces abundant $[M-H+2Li]^+$ ions that, when subjected to high-energy collisional activation (CA), undergo charge-remote fragmentations, generating a characteristic pattern of product ions [see the collisionally activated decomposition (CAD) spectrum in Figure 1A]. An interruption in the array of peaks indicates the position of the oxo group (Figure 1). Two intense peaks border or frame the gap. One peak corresponds to a product ion resulting from C–C bond cleavage β to the oxo position on the side proximal to the charge site (we call this a β ion), whereas the other is from cleavage γ to the oxo position on the side distal to the charge site (called a γ' ion). We propose structures for the β and γ' ions in Scheme I. Similar product-ion spectra were obtained with a three-sector instrument except the resolving power was poorer (spectra not given).

Most product ions form by the 1,4-hydrogen elimination mechanism (eq 1) and have a closed-shell configuration except those generated near a functional group or at either end of the chain. Examples are the ions of m/z 72, 86, and 100, which are formed by homolytic cleavage to give presumably distonic ions. The decreasing tendency for homolytic cleavage with the increase of the number of C–C bonds between the charge and the radical site may be due to the lower ability of the charge and radical sites to interact and be stabilized, arguing for true charge-remote processes at sites distant from the charge site. So far, the biggest separation between charge and radical of a stable straight-chain distonic ion involves four carbon atoms, as discussed by Kenttämaa and co-workers [16], but high-energy CAD may produce distonic ions with even greater separation in systems such as those studied here.

We currently do not understand the unsymmetrical appearance of peaks around the gap if a charge-remote 1,4-hydrogen elimination mechanism pertains because that mechanism should require that γ and γ', β and β',

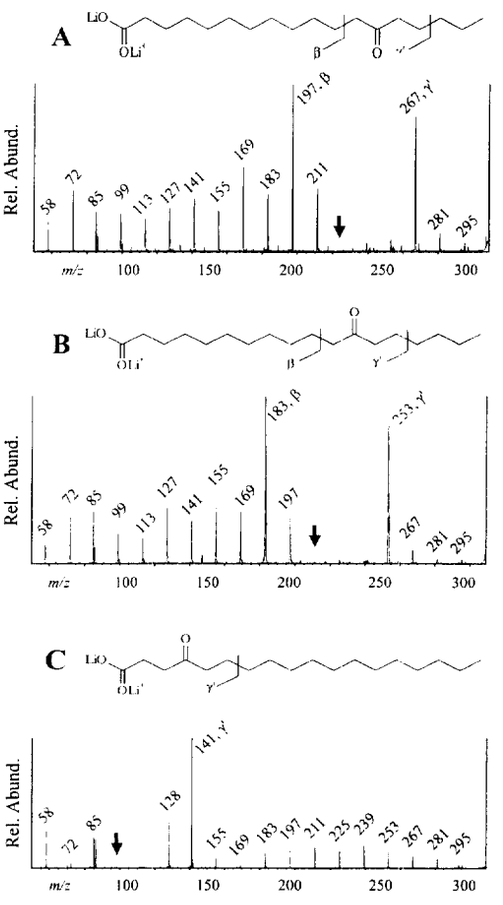

Figure 1. CAD spectra of isomeric oxofatty acids charged with Li^+ as $[M-H+2Li]^+$. The arrows indicate a point in the spectrum corresponding to the location of the oxo group. (**A**) 13-oxo-, (**B**) 12-oxo-, and (**C**) 4-oxooctadecanoic acid (m/z 311).

or α and α' ions have similar abundances. The high abundance of the γ' ion is due to the stability of α,β-conjugated system (Scheme I). A neutral analog of the McLafferty rearrangement explains the formation of the β ion, but one would expect this process to occur also on the side of the oxo group that is distal to the charge. The resulting β' ion, however, is of very low abundance. We are investigating the mechanism in ongoing studies.

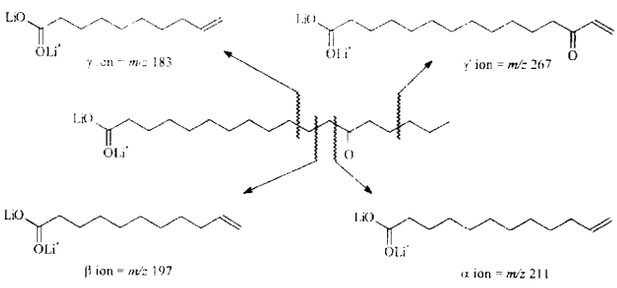

Scheme I. Formation of ions near the keto group as exemplified by dilithiated 13-oxooctadecanoate (m/z 311).

CAD of Isomeric Cationized Oxofatty Acids

Although one has difficulty distinguishing isomers such as 12- and 13-oxooctadecanoic acids by NMR or optical spectroscopy, we can easily distinguish them by their CAD spectra (Figure 1). The CAD spectrum of dilithiated 12-oxooctadecanoate (Figure 1B) has a gap after the peak corresponding to the ion of m/z 197 and two high-intensity peaks corresponding to γ' and β ions at m/z 253 and m/z 183, respectively. The spectrum of dilithiated 13-oxooctadecanoate (Figure 1A), on the other hand, gives a gap after the peak corresponding to the ion of m/z 211 and two high-intensity peaks corresponding to γ' and β ions at m/z 267 and m/z 197, respectively. The spectrum of dilithiated 4-oxooctadecanoate (spectrum 1C) gives the expected peak corresponding to the γ' ion at m/z 141 and a gap after the peak corresponding to the ion of m/z 85, but it is not possible to form a β ion from this structure. The high-energy CAD spectra of isomeric dilithiated 7- and 13-oxotetracosanoates (spectra not illustrated) are also distinct because the gap positions are different and are framed by intense peaks corresponding to γ' ions (for 7-oxo, m/z 183 and for 13-oxo, m/z 267).

CAD Spectra of Fatty Acids With an Oxo Group Near a Terminus

One of the two characteristic β and γ' ions cannot form when the oxo function is near either end of the chain (Figure 2) as for dilithiated 2-oxotetradecanoate, for which a β ion cannot form, and dilithiated 10-oxoundecanoate, for which a γ' cannot form. In order that both β and γ' ions may form, the oxo group must be located at least four C–C bonds from the carboxylate and three C–C bonds from the hydrocarbon end. Fortunately, we observe peaks corresponding to at least one of these ions together with a gap in every spectrum that we measured, allowing one to determine the oxo-group position even for fatty acids that cannot form both β and γ' ions. The peak that is 28 u higher than that corresponding to the γ' ion is always of low intensity (note the peaks at m/z 141 in Figure 2A, and at m/z 169 in Figure 1C).

When the oxo group is close to the positive-charge site, radical cations form by cleavage of the β' bond, for example, ions of m/z 128 (Figure 1C) and 100 (Figure 2A). These ions, we propose, are distonic with the radical delocalized onto the carbonyl. CA of $[M+Met]^+$ ions of *p*-hexadecanoacetanisidine, *N*-[(2-methylamino)ethyl]-2-oxononadecanamide, and 7-oxotetracosanoic acid (not illustrated) also gives these ions.

Two Competing Charge-Remote Processes

An interesting feature in the spectra of $[M-H+2Li]^+$ ions of oxofatty acids is the series of small peaks between adjoining major peaks of the regular charge-remote series (labeled with triangles in Figure 2B). We

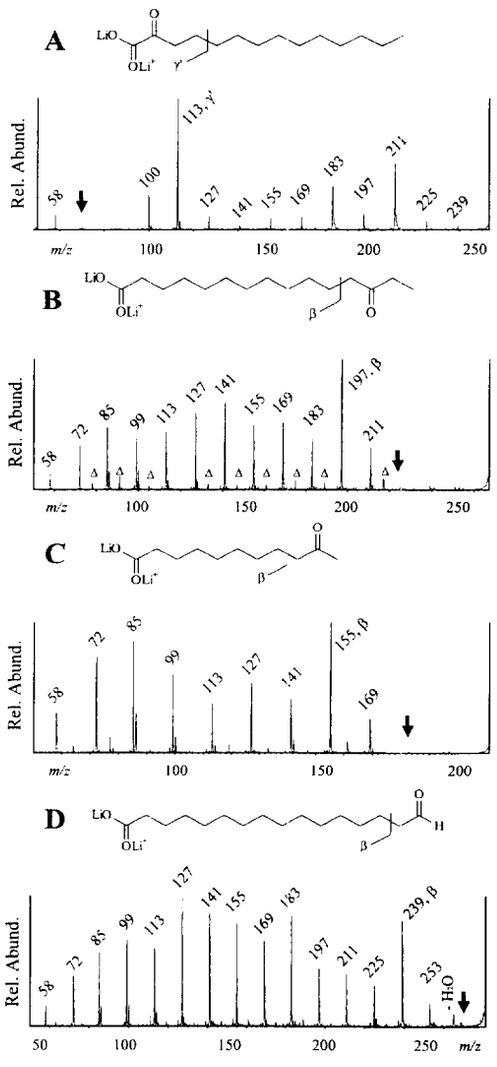

Figure 2. CAD spectra of dilithiated oxofatty acids with the oxo group near one terminus or the other. (**A**) 2-oxotetradecanoic (m/z 255); (**B**) 13-oxopentadecanoic (m/z 269); (**C**) 10-oxoundecanoic (m/z 199); and (**D**) 16-oxohexadecanoic acid (m/z 283).

propose the small peaks correspond to ions that are generated from an $(M+2Li-H)^+$ species that has one lithium attached to the oxo group and the other to the carboxylate. The decompositions are also charge remote but give rise to another pattern corresponding to ions (we call it the minor pattern) of the general composition of $C_nH_{2n-2}C{=}OLi^+R$, where R is an alkyl group. The weakness of the minor pattern suggests that the lithium affinity of –COOLi is greater than that of a ketone (to be addressed later by ab initio calculations).

CA of an $[M+Li]^+$ of an ester (methyl 12-oxooctadecanoate) gives a clearer view of the two patterns of fragmentations because the ester functional group cannot bind strongly two lithiums and competes less favorably for a single lithium ion than does –COOLi. The CAD spectrum shows a composite pattern. The most intense peak in the minor pattern corresponds to an ion that has a conjugated enone structure just like its

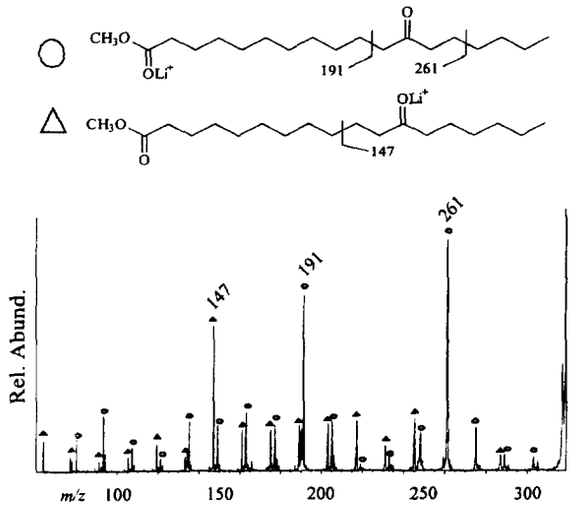

Figure 3. CAD spectrum of methyl 12-oxooctadecanoate (m/z 319). Ions labeled with a circle are the major pattern ions and those labeled with a triangle are the minor pattern ions. See text and Scheme II for detailed explanations.

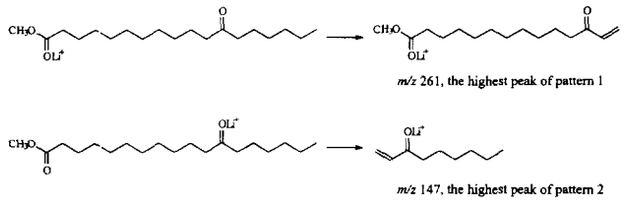

Scheme II. Formation of two competing patterns of charge-remote fragmentations as exemplified by monolithiated methyl 12-oxooctadecanoate (m/z 319).

counterpart in the major pattern, the γ' ion (Figure 3 and Scheme II). The ions of m/z 147, 161, 175, etc. correspond to peaks of a minor pattern and have a common formula, $H_2C{=}CH(CH_2)_n{-}COLi{-}C_6H_{13}$ (where n = 1, 2, 3, etc). There are lower mass members of this homologous series containing the ion of m/z 147; they presumably form by double cleavage/rearrangements. Interestingly, low-mass radical cations are produced by homolytic cleavages from the precursor ion that binds Li^+ at the ketone; examples are the ions of m/z 64 and 78, which presumably have the distonic structures, $HCOLi^+CH_2^{\cdot}$ and $HCOLi^+CH_2CH_2^{\cdot}$, respectively.

CA of an $[M+Na]^+$ of the same ester also produces a CAD spectrum that show two patterns of fragmentations (not illustrated) similar to those produced from $[M+Li]^+$, although the series derived from the precursor where Na^+ has bound at the ketone is somewhat weaker.

We sought to elucidate the nature of the competition between the two charge-remote fragmentations with ab initio calculations (see Table 1). We hypothesize that the abundance of a set of charge-remote fragments is proportional to the metal-ion affinity of the site, which is a measure of how well the charge is "fixed." The Li^+ affinity of the ester moiety, modeled by Li^+ attachment to methyl formate, and of the ketone, modeled by Li^+ attachment to formaldehyde are 39.9 and 34.2 kcal/mol, respectively. The small differences in enthalpic energy between the ester and the oxo functions, 5.7 kcal/mol, and the range of energies imparted to the ions by the

Table 1. Calculated and experimental metal-ion affinities[a]

Model reactant (M)	Cation (Met^+)	Detachment energy D_E(eV)[b]	Affinity, PCat (kcal/mol)[c]	
			Calculated	Experimental[d]
Formaldehyde (HCHO)	H^+	7.23	167.2	170.6
	Li^+	1.46	34.2	
	Na^+	1.03	24.3	
Formate$^-$ ($HCOO^-$)	H^+	14.79	341.6	346
	Li^+	7.24	167.7	
	Na^+	6.18	143.1	
(Formate$^-$ + H^+) (HCOOH)	H^+	7.54	174.5	177.5
	Li^+	1.54	36.1	
	Na^+	1.06	25.0	
(Formate$^-$ + Li^+) ($HCOO^-Li^+$)	H^+	9.09	210.1	
	Li^+	2.10	49.0	
(Formate$^-$ + Na^+) ($HCOO^-Na^+$)	H^+	9.67	223.5	
	Na^+	1.69	39.7	
Methyl formate ($HCOOCH_3$)	H^+	7.96	184.2	187.2
	Li^+	1.70	39.9	
	Na^+	1.18	27.8	

[a]Calculations were performed for all species involved in the attachment reaction: $M+Met^+ \rightarrow [M+Met]^+$. Final energies and geometries were calculated at the level of MP2(Full)/6-311+G(2d,p) [14b]. Zero-point energy, vibrational frequencies, and geometry of each multiatomic species was calculated at the level of MP2(Full)/6-31+G(d) [14b]; the values were used after scaling [15] to calculated corrected energies. ΔE_c, from the final energies. The lowest energy conformers of each species were used in reaction calculations.

[b]Detachment energy is the negative of the corrected energy for the attachment reaction (negative of the attachment energy): $D_E = -[\Delta E_c([M+Met]^+) - \Delta E_c(M) - \Delta E_c(Met^+)]$.

[c]Cation affinity, PCat, is defined as the negative of the enthalpy of the attachment reaction: $PCat = -[\Delta_f H([M+Met]^+) - \Delta_f H(M) - \Delta_f H(Met^+)]$, which was calculated by using the assumption of an ideal gas and the corrected energies of all species.

[d]All experimental values taken from [17] or [18].

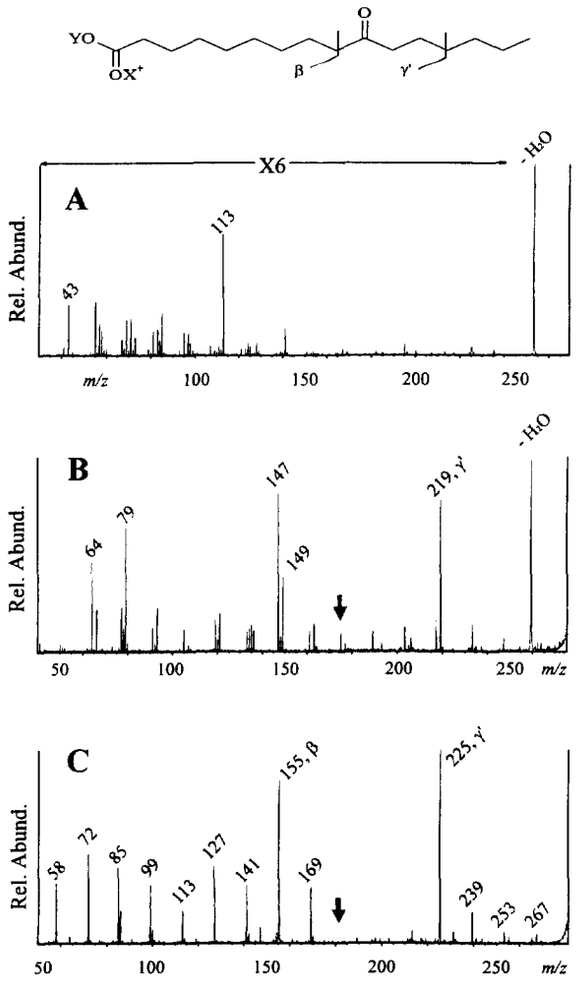

Figure 4. CAD spectra of 10-oxohexadecanoic acid with and without lithium metal ions: (**A**) protonated, X = Y = H (m/z 271); (**B**) monolithiated, X = Li and Y = H (m/z 277); and (**C**) dilithiated, X = Y = Li (m/z 283).

desorption process make it possible for the two precursors structures to coexist and for each to contribute to the fragmentation pattern. For dilithiated oxofatty acids, the affinity of the carboxylic salt for a second Li^+, modeled by Li^+ attachment to lithium formate, is 49.0 kcal/mol, which is 14.8 kcal/mol greater than that of the ketone. This larger difference in energy explains the predominance of fragmentation of a species in which the charge is localized as $-COOLi_2^+$ over that of a species in which the charge exists as a lithiated ketone when the $[M-H+2Li]^+$ of the oxofatty acid is selected.

Comparison of CAD Spectra of $[M+H]^+$, $[M+Li]^+$, and $[M-H+2Li]^+$

CAD spectra of protonated oxofatty acids, $[M+H]^+$, are not distinctive and do not allow the position of the oxo group to be elucidated. In the spectrum of the $[M+H]^+$ of 10-oxohexadecanoic acid (Figure 4A), we see only one abundant fragment, the $[M+H-H_2O]^+$ ion (the abundance of the m/z 113 ion is magnified by 6 times). The precursor ion, $[M+H]^+$, probably exists as two structures: one in which the H^+ attached to the carboxylic acid and the other which has H^+ attached to the carbonyl in the chain. Although the protonated keto is the more stable species (proton affinity of propionic acid is 190.8 kcal/mol, whereas that of acetone is 194.2 kcal/mol [17]), the loss of water probably arises from the species in which the carboxylic acid is protonated. Evidence is that protonated acids without an oxo group lose water [6], whereas protonated ketones do not [19]. The other fragments are mainly carbocations and are formed either from the $[M+H]^+$ or the $[M+H-H_2O]^+$.

Activation of the $[M+Li]^+$ ion of the same acid causes fragmentation by various pathways (Figure 4B). The $[M+Li-H_2O]^+$ is evident presumably because the terminal OH group may easily abstract a proton to give $-CO-OH_2^+$, which loses H_2O. Small cations are also formed by charge-mediated processes. Like the $[M+Li]^+$ ion of methyl 12-oxooctadecanoate, the $[M+Li]^+$ ion of 10-oxohexadecanoic acid fragments to give two patterns of fragment ions. Because the Li^+ affinity of formic acid is 36.1 kcal/mol, whereas that for formaldehyde is 34.2 kcal/mol (Table 1), comparable populations of both charged species exist and fragment, giving two patterns of comparable intensities.

When two lithium ions are used to cationize the same acid (Figure 4C), charge-remote fragmentations become predominant. As discussed earlier, the difference in energy between attachment of Li^+ to the carboxylic salt and to the ketone is 14.8 kcal/mol, favoring the $-COOLi_2^+$ and its fragments. The loss of H_2O is suppressed because the OH now exists as OLi. These precursor ions are the preferred source of structure information.

CAD of Oxofatty Acids Charged with Different Alkali Metal Ions

The CAD spectra of 10-oxohexadecanoic acid that is cationized by different alkali metal ions are very similar (Figure 5). Although only the CAD spectra of disodiated and dirhubidiated species are shown in Figure 5, those of dipotassiated and dicesiated species contain the same characteristic features. Common to all spectra are three inorganic ions: the free metal cation that was used for cationization, the ionized metal dimer $Met_2^{+\cdot}$, and the $Met_2O^{+\cdot}$ [6].

The oxofatty acids charged with heavier alkali metal ions also undergo charge-remote fragmentation but principally of the $-COOMet_2^+$ species. The capability to use alternative alkali metal ions provides some advantages in problem solving because the choice of metal determines whether there is one or two series of charge-remote fragments. With the heavier metals, the metal ion affinities of both the carboxylate and carbonyl are weakened because the metal ion is of greater size, but metal-ion bonding to the isolated carbonyl becomes so

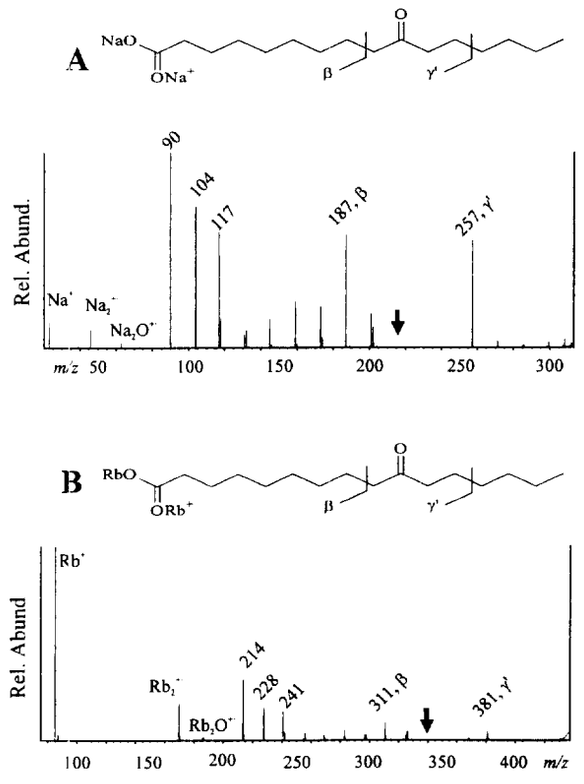

Figure 5. CAD spectra of 10-oxohexadecanoic acid cationized with different alkali metals: (**A**) with sodium iodide (m/z 315) and (**B**) with rhubidium iodide (m/z 439).

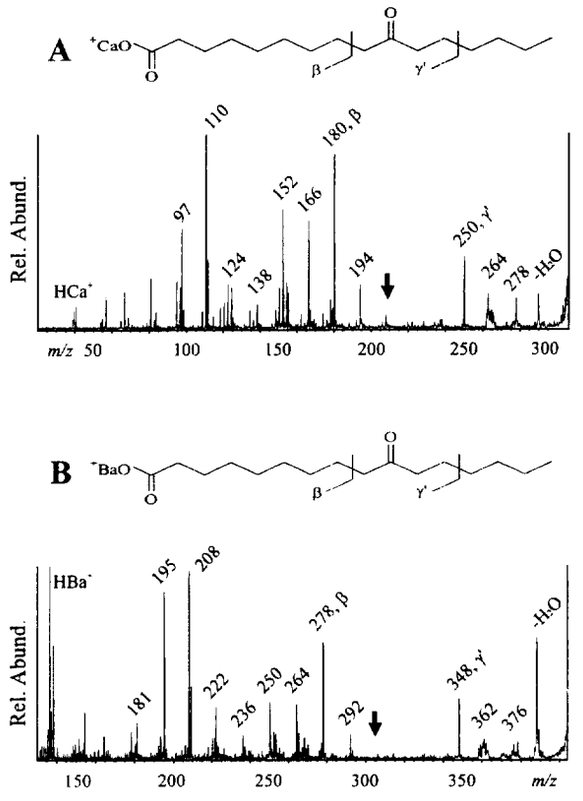

Figure 6. Comparison of CAD spectra of 10-oxohexadecanoic acid cationized with different alkaline earth metal ions: (**A**) with $CaCl_2$ (m/z 308) and (**B**) with $BaCl_2$ (m/z 406).

labile that the metal ion is released as Met^+ upon activation, preempting fragmentation remote to that charge site. For example, the Na^+ affinities of the ketone carbonyls and the sodium carboxylates, modeled by Na^+ attachment to formaldehyde and sodium formate are 24.3 and 39.7 kcal/mol, respectively (Table 1). The sodium attachment to the ketone carbonyl is too weak to allow charge-remote fragmentation to compete with metal-ion ejection, unlike sodium attachment to the carboxylate. The larger alkali metal ions are bound even more weakly, allowing metal-ion ejection to be more facile (Figure 5). Second, if the precursor ion overlaps with another from the background or an impurity, switching to a different metal often removes that overlap and allows a noncomposite spectrum to be obtained. For example, in the CAD spectrum of dipotassiated 10-oxohexadecanoic acid, there was an unexpected fragment of m/z 194. By comparing the spectra obtained by using different metal ions, we confirmed that the m/z 194 ion was from a contaminant.

CAD of Oxofatty Acids Charged with Alkaline Earth Metal Ions

In general, the CAD spectra of $[M-H+Met]^+$ of oxofatty acids, where *Met* is an alkaline-earth metal ion, are similar to those for acids bound to alkali metal ions and allow the oxo position to be located readily. CAD spectra of 10-oxohexadecanoic acid charged with Ca^{2+} or Ba^{2+} (Figure 6) contain nearly the same information as those of the compounds charged with Mg^{2+} or Sr^{2+}.

The CAD spectra of oxofatty acids charged with alkaline earth metal ions are not as distinctive as those charged with alkali metal ions, suggesting that binding of *one* alkaline earth metal ion to a carboxylate is less strong than that for *two* alkali metal ions. Additional evidence is the H_2O loss from the precursor ions to give ions of m/z 290 in Figure 6A and m/z 388 in Figure 6B.

CAD of Carboxylates in the Negative Ion Mode

The simplest way to fix the "charge" on a fatty acid is to remove a proton from the –COOH function. The negatively charged species is either a carboxylate or an enolate. The latter is less likely, however. Given that the charge is at the acid end, there should be no competing patterns in the charge-remote fragmentation of anions. We demonstrate, in Figure 7, that this is the case.

Generally, the CAD spectra of carboxylates look similar to those of their positive metal-cationized counterparts. There are low-mass radical anions in these and other CAD spectra of fatty acid carboxylates that are worthy of note because previous studies were not done under the good mass resolving power used here. A common pair is of m/z 71 and 72: the structure of the

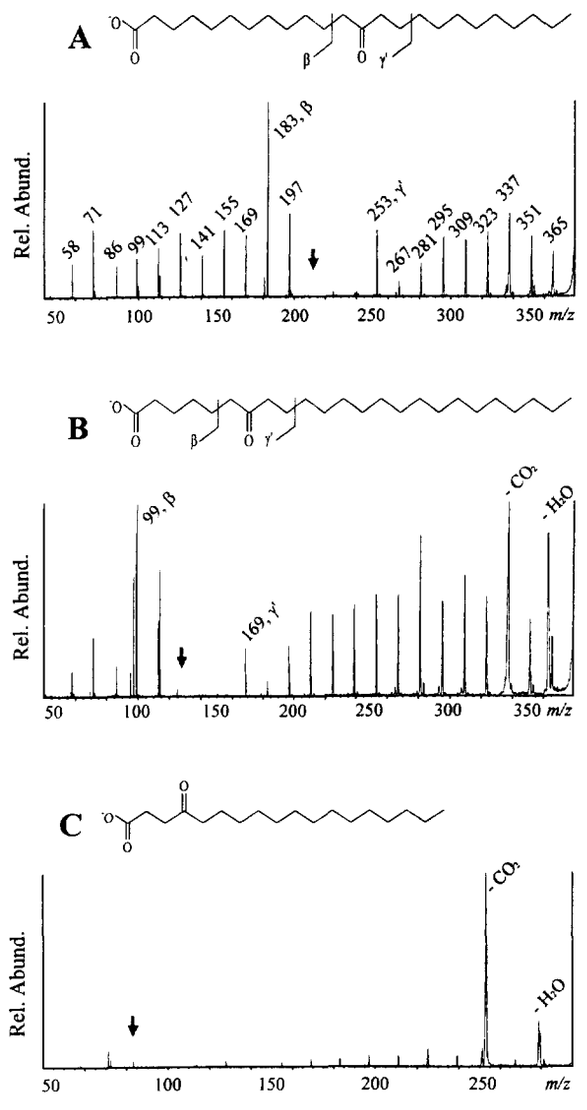

Figure 7. CAD spectra of (**A**) 13-oxotetracosanoate (m/z 381), (**B**) 7-oxotetracosanoate (m/z 381), and (**C**) 4-oxooctadecanoate (m/z 297).

m/z 72 ion is likely to be distonic ($\dot{C}H_2CH_2COO^-$), whereas that of m/z 71 is a closed-shell species, $CH_2{=}CHCOO^-$. One expects that the next higher mass ion would be of m/z 85, having a structure of $CH_2{=}CHCH_2COO^-$, but instead we see an ion of m/z 86, which is likely to be either a distonic anion ($\dot{C}H_2CH_2CH_2COO^-$) or a cyclic lactone radical anion [3]. The relative stability of distonic radical anions decreases with an increase in the distance between the radical and the anion sites. Doublets are rarely seen after m/z 113 and 114, underscoring the diminishing stability of α,ω-distonic ions.

CAD spectra of carboxylates are usually as structurally distinctive as those of positive species. The oxo position on the chain is indicated by the spectrum gap (Figure 7), and peaks due to the β and γ' ions are, as expected, of high intensity. Isomers are readily distinguished from each other by the different positions of the gap that is framed by the β and γ' ions (Figure 7A and 7B).

There are small differences between positive and negative-ion CAD patterns. First, the relative abundance of γ' ions is less in the negative-ion mode. Second, the ion 14 u higher than the γ' ion in the negative-ion spectrum is of very low abundance (compare ions of m/z 267 in Figure 7A and of m/z 183 in Figure 7B). For positive ions, on the other hand, it is the ion 28 u higher than the γ' ion that is of low abundance (compare ions of m/z 141 in Figure 2A and of m/z 169 in Figure 1C). We do not have an explanation for these phenomena. Third, we see long-chain distonic radical cations but not distonic radical anions of comparable size. For example, dilithiated 7-oxotetracosanoic acid (spectrum not shown) undergoes cleavage of the bond β to the carbonyl at the distal side to form a long chain distonic ion, $^+Li_2OOC(CH_2)_5\dot{C}OCH_2^{\cdot}$ (m/z 170), whereas we cannot detect the corresponding anion, $^-OOC(CH_2)_5\dot{C}OCH_2^{\cdot}$ (of m/z 156) (Figure 7B). The negative charge may stabilize the radical site less than the positive charge. Fourth, the negative-ion CAD spectra are "cleaner" in the low-mass range because no ions below m/z 58 are able to form, and no metal ions can be ejected.

A disadvantage of CAD of carboxylates is that they tend to lose H_2O and CO_2 to form carbanions when a functional group is nearby. The closer the carbonyl is to the carboxylate, the greater the loss of H_2O and CO_2. The CAD spectrum of 7-oxotetracosanoate, for example, indicates the location of the oxo group by the position of the gap, although the fragments of $[M-H-H_2O]^-$ and $[M-H-CO_2]^-$ (of m/z 363 and 337, respectively) are predominant. On the other hand, the CAD spectrum of 4-oxooctadecanoate provides little structural information (Figure 7C) because the $[M-H-H_2O]^-$ and $[M-H-CO_2]^-$ ions (of m/z 279 and 253) are extraordinarily abundant, indicating an interaction between the carbonyl and the carboxylate.

Conclusions

Collisional activation of oxofatty acids, which are desorbed as carboxylates or as metal-ion cationized species, leads to charge-remote fragmentations that provide information about the oxo position in the chain. The generality of the fragmentation has been established by the study of more than ten fatty acids with various oxo positions and different chain lengths. Unlike many other functional groups that can be located by charge-remote fragmentations, the oxo group provides another binding site for the second alkali metal ion. Therefore, there are two series of fragment ions when a lithiated species is activated because the lithium-oxo bond energy is sufficient to survive high energy activation, thereby "fixing" the charge. For larger alkali metals, the metal/keto bond is weak, and the metal ion is simply ejected from the molecule upon collisional activation. The extent of competition is understandable

in terms of metal-ion affinities, which were calculated by ab initio methods, and can be controlled by metal-ion selection.

This charge-remote chemistry will be useful for determining the structure of unusual fatty acids and related materials, such as that encountered in our recent study of lipid materials from a marine organism [11]. Moreover, the fragmentation mechanism should provide insight on charge-remote processes in general, and these studies are underway. Of principal interest is the unsymmetric pattern in the region of the gap, a subpattern that appears to be at odds with the concept of "charge remote."

Acknowledgment

This research was supported by the National Institutes of Health Center for Research Resources (Grant No. 2P41-RR-00954).

References

1. (a) Tomer, K. B.; Crow, F. W.; Gross, M. L. *J. Am. Chem. Soc.* **1983,** *105,* 5487–5488; (b) Adams, J. *Mass Spectrom. Rev.* **1990,** *9,* 141–186; (c) Gross, M. L. *Int. J. Mass Spectrom. Ion Proc.* **1992,** *118/119,* 137–165.
2. Davoli, E.; Gross, M. L. *J. Am. Soc. Mass Spectrom.* **1990,** *1,* 320–324.
3. Jensen, N. J.; Tomer, K. B.; Gross, M. L. *J. Am. Chem. Soc.* **1985,** *107,* 1863–1868.
4. Cordero, N. N.; Wesdemiotis, C. *Anal. Chem.* **1994,** *66,* 861–866.
5. Adams, J.; Gross, M. L. *J. Am. Chem. Soc.* **1986,** *108,* 6915–6921.
6. Adams, J.; Gross, M. L. *Anal. Chem.* **1987,** *59,* 1576–1582.
7. Jensen, N. J.; Tomer, K. B.; Gross, M. L. *Anal. Chem.* **1985,** *57,* 2018.
8. Determing, L. J.; Gross, M. L. *Anal. Chim. Acta* **1987,** *200,* 431.
9. Crockett, J. S.; Gross, M. L.; Christie, W. W.; Holman, R. T. *J. Am. Soc. Mass Spectrom.* **1990,** *1,* 183–190.
10. Murphy, R. C. In *Handbook of Lipid Research 7: Mass Spectrometry of Lipids;* Snyder F., Ed.; Plenum: New York, 1993, p 213.
11. Fu, X.; Abbas, S. A.; Schmitz, F. J.; Govindan, M.; Hanson, K. M.; Horton, O. A.; Crews, O.; Vidavsky, I.; Gross, M. L.; Laney, M.; Schatzman, R. C.; Cabuslay, R. D. *Tetrahedron* **1997,** *53,* 799–814.
12. Gross, M. L.; Chess, E. K.; Lyon, P. A.; Crow, F. W.; Evans, S.; Tudge, H. *Int. J. Mass Spectrom. Ion Phys.* **1982,** *42,* 243–254.
13. Gross, M. L. In *Methods in Enzymology;* McCloskey, J. A., Ed.; Academic: San Diego, CA, 1990; Vol. 193, pp 131–153.
14. (a) Frisch, M. J.; Trucks, G. W.; Schlegel, H. B.; Gill, P. M. W.; Johnson, B. G.; Robb, M. A.; Cheeseman, J. R.; Keith, T.; Petersson, G. A.; Montgomery, J. A.; Raghavachari, K.; Al-Laham, M. A.; Zakrzewski, V. G.; Ortiz, J. V.; Foresman, J. B.; Cioslowski, J.; Stefanov, B. B.; Nanayakkara, A.; Challacombe, M.; Peng, C. Y.; Ayala, P. Y.; Chen, W.; Wong, M. W.; Andres, J. L.; Replogle, E. S.; Gomperts, R.; Martin, R. L.; Fox, D. J.; Binkley, J. S.; Defrees, D. J.; Baker, J.; Stewart, J. P.; Head-Gordon, M.; Gonzalez, C.; Pople, J. A. *Gaussian 94,* Revision D.3, Gaussian, Inc., Pittsburgh, PA, 1995; (b) Frisch, M. J.; Frisch, A.; Foresman, J. B. in *Gaussian 94,* User's Reference, Gaussian, Inc., Pittsburgh, PA, 1995, and references therein.
15. Pople, J. A.; Scott, A. P.; Wong, M. W.; Radom, L. *Isr. J. Chem.* **1993,** *33,* 345–350.
16. Smith, R. L.; Chyall, L. J.; Chou, P. K.; Kenttamaa, H. I. *J. Am. Chem. Soc.* **1994,** *116,* 781–782.
17. Hunter, E. P.; Lias, S. G. "Proton Affinity Evaluation," in *NIST Standard Reference Database 69;* Mallard, W. G.; Linstrom, P. J., Eds. National Institutes of Standard and Technology, Gaithersburg, MD, 1997 (http://webbook.nist.gov)
18. Caldwell, G.; Renneboog, R.; Kebarle, P. *Can. J. Chem.* **1989,** *67,* 661.
19. Harrison, A. G. *Chemical Ionization Mass Spectrometry;* CRC: Boca Raton, FL, 1992, p 140.